Crack opening conditions at 'corner nodes' in FE analysis with cracking along mesh lines

Daniela Ciancio, Ignacio Carol, Massimo Cuomo

Crack opening conditions at 'corner nodes' in FE analysis with cracking along mesh lines

Daniela Ciancio [a], Ignacio Carol [a], Massimo Cuomo [b]

[a] *Technical University of Catalonia (UPC), Department of Geotechnical Engineering and Geo Sciences, Carrer/Jordi Girona 1 3, 08034, Barcelona, Spain*

[b] *University of Catania, Department of Civil and Environmental Engineering, Viale Andrea Doria 6, 95125, Catania, Italy*

Abstract

On the basis of a recent work proposed by the authors on a double minimization method for evaluating inter element forces and stresses transmitted across mesh lines, the crack opening conditions at a corner node of the FE mesh, from where several lines (potential cracks) emanate, is examined in this paper. The study is developed locally as a post process ing step of a standard displacement based FE calculation, in terms of an always increasing external (macroscopic) load factor μ. The cracking laws for each potential crack line are assumed rigid plastic with hyperbolic failure criterion in terms of normal and shear components of the stress traction at that point. It is observed that, as μ increases, in general such point may undergo up to four phases of evolution until a crack can effectively open through it. First, while stress tractions across mesh lines at the point are all below cracking criterion, forces may be evaluated with the double minimization method recently proposed. Second, cracking criterion is reached for one of the lines only. Stress evaluation requires a modified minimization method with one (hyperbolic) constraint; however, crack still does not open at the node because of the lack of kinematic continuity. Third, cracking criterion is satisfied for a second of the lines converging at the nodal point. Stress tractions may then be calculated with a system of equations involving the two hyperbolic constraints alone and no min imization is needed. But in general the through crack cannot open yet at this stage because of non coincident flow rules, until either (i) a third line reaches the cracking criterion, or (ii) these get reoriented to exhibit parallel directions in the glo bal reference system. Two simple examples of application are provided which illustrates the development of the various cracking stages and shows different situations that may take place.

Keywords: Fracture analysis; Rigid fracturing interface; Inter element forces; Concrete fracture

1. Introduction

A number of methods and techniques have been proposed in the literature for the FE analysis of the cracking and fracture behavior of quasi-brittle materials such as concrete, rock, ice, ceramics, etc. Since

Nomenclature

$\mathbf{t}$	traction vector
σ	normal stress component
τ	shear stress component
F	fracture surface function
p	parameters of F
$\mathbf{w}$	interface opening displacement
λ	plastic multiplier
$\mathbf{m}$	flow rule direction vector
Q	potential surface
n, s	interface local reference system
x, y	global reference system
H	softening parameter
$\mathbf{C}^{\tan}$	tangential compliance matrix
c	asymptotic cohesion
χ	tensile strength
ϕ	asymptotic friction angle
$G_{\mathrm{f}}^{\mathrm{I}}$	mode I fracture energy
$G_{\mathrm{f}}^{\mathrm{IIa}}$	mode IIa fracture energy
W^{cr}	dissipative energy
$\mathbf{B}$	matrix containing the derivatives of the shape functions
$\mathbf{f}$	nodal element force
$\mathbf{r}$	nodal inter-element force
Ω	contributing area
$\mathbf{Q}$	rotation matrix
Φ	objective function
$\mathbf{T}$	stress tensor
$\mathbf{r}$	arbitrary inter-element force
$\mathbf{D}$	2×2 matrix
$\mathbf{d}$	2-row vector
μ	external loading factor
Δ	finite increment
E	Young modulus
V	Poisson modulus

Superscript
(i), (k), (l) referring to the ith, kth and lth interface

the pioneering work in the 60s [1], methods that followed based on both of the ''smeared crack approach'' and ''discrete crack approach'' types [2–5], exhibited a variety of advantages and shortcomings.

The original discrete approach methods based on linear elastic fracture mechanics (LEFM) [6] first and then also non-linear fracture mechanics (NLFM) [7] proposed a physical representation of the evolution of individual cracks at the expense of onerous analysis due to repetitive remeshing processes. Furthermore, the possible applications were limited by structural scale conditions, one or two cracks maximum could develop simultaneously, and the determination of the propagation direction of the crack and its length were aspects not totally solved.

On the other hand, methods based on the smeared approach, using a fixed mesh of continuum elements and standard continuum-type constitutive equations with softening, also thrived at identifying macrocrack direc-

tion among the cloud of ''cracking'' Gauss points obtained, often in chaotic state of stress and strain involving thick element bands or even substantial parts of the structure (see for instance [4,5]).

More modern techniques, such as XFEM and SDA, also require the identification of a crack path line using the so-called ''tracking algorithm'', which still appears as an ad hoc procedure independent (or at least detached) from the fundamental principles of mechanics which govern the continuum behavior, and are also intrinsically limited to handling problems with one or two (or in any case very few) simultaneous propagating cracks [8,9].

An intermediate approach proposed very early, but developed more efficiently only since the 90s as computer power became commonly available [10 14], is that of considering each line in the mesh as a potential crack, evaluating inter-element forces and stresses, and allowing crack opening/sliding along those same lines as appropriate strength criteria are exceeded. Although not free of shortcomings (e.g. cracks can only develop along the initial mesh lines), at least these methods have provided a means of describing crack propagation in a fully automatic and fully integrated way with the rest of the mechanical problem, eliminating completely the need of tracking or remeshing and without any limitations on how many cracks open, close, reopen, branch or bridge.

This approach has been implemented mainly in two ways. One uses in a systematic fashion the so-called zero-thickness interface elements with double nodes. These elements are inserted along each line of the mesh (or along a carefully chosen subset of them) so that all possible fracture patterns to be considered are ''built into'' the FE mesh from the beginning of the analysis [13]. Initially, the interface elements are assigned a very high elastic stiffness in order not to add spurious compliance to the structure but on the other hand be able to provide the stress tractions σ, τ transmitted. When a given cracking criterion is exceeded, a fracture-based interface constitutive law is activated, leading to energy-driven crack opening predictions. Such constitutive laws do normally exhibit elasto-plastic structure of the work-softening type, and may be considered as mixed-mode generalizations of the cohesive crack models by Dugdale or Hillerborg [15,16]. This approach has led to very realistic predictions of cracking and fracture mechanisms under complex stresses in 2D and more recently also in 3D [17], involving multiple cracks which start, get connected, arrested, bridge or branch with other cracks, etc. all in a completely spontaneous manner. On the negative side, this implementation requires a large number of nodes, limiting severely the maximum problem size that can be analyzed for given computer resources.

The second way for implementating this approach is to avoid the use of interface elements and only duplicate nodes along those lines for which cracking conditions are exceeded, therefore saving many nodes, reducing the problem size, and eliminating the non-physical compliance introduced by interface elastic behavior and the potential ill-conditioning problems associated to its high stiffness values. However, among other things, this type of implementation requires to evaluate the inter-element forces (or stress tractions between elements) from the results of a standard FE analysis which, as simple as it may sound, turns out not a trivial problem and may be ill-defined at the corner nodes in 2D or at the corner and edge nodes of elements in 3D. This may explain why the existing approaches of this type in 2D have been traditionally based on inter-element force evaluation and crack verification at the mid-side nodes of quadratic element sides, only location at which the computation of such forces becomes trivial [11,18].

As a first ingredient of a general ''interface-free'' formulation of discrete cracking along mesh lines, in which conditions could be checked also (and mainly) at ''element corner nodes'', the authors have recently proposed a new procedure to evaluate the inter-element forces and stresses at the nodal ends of mesh lines [19]. The procedure, inspired on the concepts of microplane model [20,21], is based on a double minimization of the stress tractions along all mesh lines emanating from a corner node, with respect to a Mohr circle representing the ''true'' or average stress state at the node. The final expressions boil down to a simple 2×2 linear system for each corner node of the mesh, whose coefficients are evaluated as a post-processing of the results of a standard linear elastic FE analysis. The solution of such system at each node not only leads to all the stress tractions along mesh lines, but as an added feature it also yields the above-mentioned average stresses at the node, and therefore it may be also used as an (advantageous and cheap) ''stress smoothing'' procedure.

In the current paper, the authors proceed forward along this line of work investigating the conditions for crack opening at an element corner node of the FE mesh. For this purpose, each mesh line emanating from the node is considered a potential crack. A failure (cracking) surface is assumed for each potential crack, in terms

of the normal and shear components of the corresponding stress traction. A flow rule is also assumed, in connection to the cracking surface, in full similarity to what is done in elasto-plastic interface constitutive models [22].

After this introduction, the paper is structured as follows: the general aspects of the study, main definitions, possible modes of cracking, cracking criterion and other assumptions are described in Section 2. In Section 3, the various stages of the process for crack opening at an element corner node are identified and formulated. For each of them, the corresponding equations are established and the solution method is proposed always as a post-processing step of a standard finite element calculation. In Section 4, two numerical examples are provided in which the cracking analysis is performed for simple rectangular meshes in which the central nodes turn out to be critical for cracking. Among other results given are the values of the external loading factor μ, for which each of the stages in the cracking process are reached at the various points in the mesh. Finally, the main results of the work described are summarized and commented in Section 5.

2. Main assumptions and equations

2.1. General

As indicated, this study is oriented to elucidate the cracking conditions at a *corner node* of a standard displacement-based FE calculation, assuming that every line of the mesh is a potential crack line. A *corner node* is understood in this context as any node which sits at the corner of an element of the mesh, as opposite to *middle nodes* that are considered in quadratic elements. Thus, in a mesh with linear elements only (3-node triangles or 4-node quadrilaters) all nodes in the mesh are corner nodes. Among corner nodes also inner and boundary nodes may be distinguished. Boundary nodes would be those sitting on the boundary of the domain, while the rest are inner nodes.

The results to be obtained in this study are intended ultimately to make possible a general non-linear calculation procedure in which a number of mesh lines may develop into cracks and, if required, the continuum elements may be also considered non-linear. However, the specific objectives of this paper are to look in detail at the cracking development process through one single corner node of the mesh, at the conditions that apply, at the various stages involved and to find how to identify at what point the node has really satisfied all necessary requirements and therefore has reached the onset of crack opening. For this purpose, and for the sake of simplicity, one can consider the continuum elements as linear elastic and all other potential cracks closed, which actually includes all the processes of interest before the first crack really opens and therefore corresponds to simple linear elastic calculation at the FE level. In this simplified conditions, the state of displacements, forces, stresses, etc. on the structure is simply characterized by a scalar loading factor μ, which scale all these quantities proportionally from the results of a single nominal load FE calculation.

2.2. Possible crack mechanisms through a corner node and FE mesh

In the most general case, the various mechanisms for the growth and propagation of a crack through a single corner node are illustrated in detail in Fig. 1. As previously mentioned, each mesh line can be interpreted as potential cracks that can open if certain fracture criteria are satisfied.

In Fig. 1a, N mesh lines converge at node A, inner node of a generic FE mesh made of triangular elements. From c to e, the duplication of the interior node A is used to simulate the propagation of the crack tip (crack tip showed in Fig. 1b), the growth and the bifurcation of the crack. One observation that arises looking at the mechanisms in Fig. 1 is that one single crack line (out of the various converging on the node) cannot open alone. The duplication of the interior node implies the opening of, at least, two of the concurring lines on that node.

The same scenarios (propagation, growth and bifurcation of a crack) of Fig. 1 are presented in Fig. 2 for a generic mesh made of triangular elements, discretizing part of a body of a fracturing material at two different times t_0 and t_1. At time t_0, nodes A and C represent the crack tips of two cracks inside the material, and node B is a point within the intact part of the material. At time t_1, the crack on the left side propagates, and node A

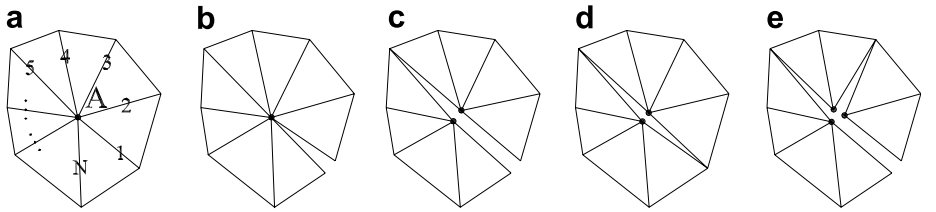

Fig. 1. (a) N mesh lines concurring at the interior node A; (b) crack tip at the interior node A; (c) crack propagation through the interior node (node duplicated); (d) crack opening through the interior node (node duplicated); (e) crack bifurcation through the interior node (node triplicated).

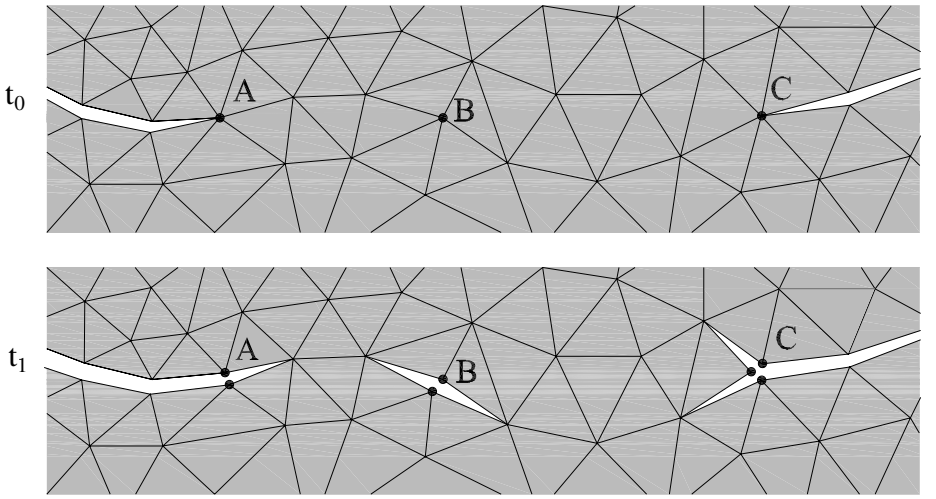

Fig. 2. At time t_0: nodes A and C are crack tips, node B is a point within the intact material; at time t_1: node A duplicates and the crack propagates, node B duplicates and a crack growthes, node C triplicates and the crack bifurcates.

duplicates. At the same time-increment, a new crack appears in correspondence with node B, that duplicates as well as node A. At time t_1 the crack on the right side bifurcates and, consequentially, node C triplicates.

2.3. Crack failure criterion and rigid-plastic model

As already indicated, all mesh lines are considered as potential cracks. In the context of this study, cracking conditions will be checked at the ends of those lines where they are connected to the corner nodes.

The failure criterion and subsequent evolution model for a crack line are very similar to previous elasto-plastic constitutive models for interfaces [22], except that elastic deformations are not present and therefore the constitutive model is of a rigid-plastic type. As such it will be defined in the following paragraphs; however, it is important to note that since this study only considers evolution until the onset of cracking at the corner node of the mesh, only the failure criterion and initial flow rule will really have a relevance in the present study.

At any point of the mesh line, and in particular at its ends where cracking conditions will be checked, consider the stress traction vector $\mathbf{t} \quad (\sigma, \tau)$ defined as the collection of normal and shear components of the stress tractions transmitted across the line. How these tractions can be computed at each stage of the analysis, is part of the formulation developed in Section 3.

The *crack failure criterion* is defined in the standard way by means of a scalar loading function of the traction $\mathbf{t}$ components $F(\mathbf{t}, \mathbf{p})$, where $\mathbf{p}$ denotes a collection of parameters which define the shape and size of the surface and that in general evolve during the cracking process. If $\mathbf{p}_0$ are the initial values of those parameters, as tractions increase two situations may be distinguished:

(1) If $F(\mathbf{t}, \mathbf{p}_0) < 0$ the potential crack is still closed.
(2) If $F(\mathbf{t}, \mathbf{p}_0)$ 0 the cracking criterion has been reached.

Note that, as in plasticity, $F > 0$ is not allowed, and that the cracking criterion $F(\mathbf{t}, \mathbf{p}_0)$ 0 is only a necessary condition for crack opening.

In the case that the crack would start to open, the opening direction will be given by a *flow rule* $\mathbf{m}$ in a way also similar to standard plasticity, that is:

$$\dot{\mathbf{w}} = \dot{\lambda}\mathbf{m} \tag{1}$$

in which $\mathbf{w}$ is the relative opening displacement of the crack, $\dot{\lambda}$ a scalar multiplier indicating the intensity of the opening, and $\mathbf{m}$ is the direction of the displacement or flow rule. This direction may be conveniently defined as the gradient of a potential surface $Q(\sigma, \tau)$:

$$m_i = \frac{\partial Q}{\partial t_i} \Rightarrow \mathbf{m} = \begin{bmatrix} \frac{\partial Q}{\partial \sigma} \\ \frac{\partial Q}{\partial \tau} \end{bmatrix} \tag{2}$$

If the cracking model is associated, then Q F. The examples and the applications reported in this paper imply the hypothesis of associated failure criterion.

Although not strictly required for the purpose of this study, the rest of the rigid-plastic crack opening model is defined for completeness. The production of irreversible opening displacements in the loading and unloading scenario are governed by the Kuhn Tucker conditions:

$$F \leqslant 0, \quad \dot{\lambda} \geqslant 0 \text{ and } F\dot{\lambda} = 0 \tag{3}$$

Opening of the crack must satisfy additionally the consistency condition:

$$\dot{F} = \mathbf{n} \cdot \dot{\mathbf{t}} - \dot{\lambda} H h = 0 \tag{4}$$

in which the normal $\mathbf{n}$ to the surface F and the hardening/softening parameter H are defined as

$$\mathbf{n} = \left.\frac{\partial F}{\partial \mathbf{t}}\right|_p, H = -\left.\frac{\partial F}{\partial \lambda}\right|_\sigma = -\frac{\partial F}{\partial \mathbf{p}} \frac{\partial \mathbf{p}}{\partial \mathbf{w}} \cdot \mathbf{m} \tag{5}$$

In this equation, it has been assumed that the evolution of the parameters is governed directly (through invariants) or indirectly (through energy dissipated) by the increments of opening displacements, as it is normally done in elasto-plastic interface models. Finally, from Eq. (5) one can isolate the inelastic multiplier $\dot{\lambda}$ and replace it into flow rule Eq. (1), to obtain the tangential compliance for the overall rigid-plastic model:

$$\dot{\mathbf{w}} = \mathbf{C}^{\tan} \cdot \dot{\mathbf{t}}; \quad \mathbf{C}^{\tan} = \frac{1}{H} \mathbf{m} \otimes \mathbf{n} \tag{6}$$

The expressions given so far refer to a generic fracture surface F. The numerical applications presented in this paper use the fracture energy based constitutive law of Carol et al. [13], the relevant ingredients of which are represented in Fig. 3 and briefly described in the following.

The initial loading (failure) surface F 0 is given as a three-parameter hyperbola with the following expression:

$$F = \tau^2 - (c - \sigma \tan\phi)^2 + (c - \chi \tan\phi)^2 \tag{7}$$

where tensile strength χ, asymptotic "cohesion" c and asymptotic friction angle ϕ are model parameters referred to as $\mathbf{p}$ in the previous formulas (Fig. 3a). Classic Mode I fracture occurs in pure tension. A second Mode IIa is defined under shear and high compression, with no dilatancy allowed (Fig. 3b). The fracture energies G_f^{I} and G_f^{IIa} are two model parameters. After initial cracking, χ, c and $\tan\phi$ decrease (Fig. 3d and e), and the loading surface shrinks, degenerating in the limit case into a pair of straight lines representing pure friction (Fig. 3c). The process is driven by the energy spent in fracture process, W^{cr}.

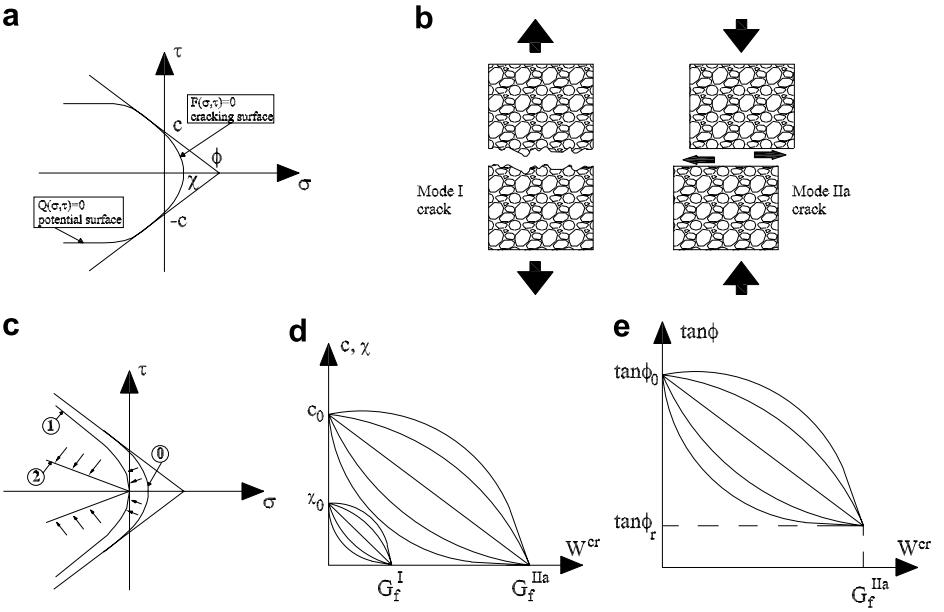

Fig. 3. Interface cracking laws: (a) hyperbolic cracking surface F and plastic potential Q; (b) fundamental modes of fracture; (c) evolution of cracking surface; (d) softening laws for χ and c; (e) softening law for $\tan\phi$.

3. Stages to the onset of crack opening and formulation

3.1. General definitions, inter-element tractions during "Stage 0"

Consider a generic corner node of the mesh and the mesh lines (potential cracks) which emanate from it, as represented in Fig. 4a. For convenience these lines are numbered counterclockwise from one of them chosen arbitrarily, from 1 to N. A local reference system of unit vectors normal and shear to each of the lines at the node is defined by $\mathbf{n}^{(i)}$, $\mathbf{s}^{(i)}$, i 1, N (also in Fig. 4a). The stress tractions transmitted across each of the lines are denoted as $\mathbf{t}^{(i)}$, i 1, N, and are represented on the right-hand side of the same figure in the Mohr's plane, in which also the cracking surface F 0 defined in terms of the normal and shear components of stress tractions on a generic plane is depicted.

Note that in Fig. 4b all mesh line tractions have been represented well inside the failure envelope. This would correspond to "stage 0" of the cracking process under study, in the sense that the cracking criterion is not satisfied for any of the mesh lines concurring at the corner node.

At this stage of the loading process, the stress tractions across each of the mesh lines, $\mathbf{t}^{(i)}$, i 1, N, are calculated as a post-processing step from the standard results of the linear elastic FE analysis, by applying a method recently developed by the authors [19], which is briefly described in the following.

Linear elastic standard FE analysis under nominal external loads leads to the values of nodal displacements, and strains and stresses at the element Gauss points. For each element, also equilibrium nodal forces may be recovered either by multiplication of the element displacement vector by element stiffness matrix, or by integration of $\mathbf{B}^t\mathbf{t}$ over the element volume. Either way, the equilibrium forces on each of the element nodes may be trivially obtained, and consequentially those forces on all the element tips converging on the "*corner node*" of Fig. 4a. The latter are denoted also as $\mathbf{f}^i$, i 1, N (the convention used is that element tip i lies between mesh lines i and $i-1$) in Fig. 5. In the same figure the *inter-element forces* transmitted between adjacent elements are also introduced and defined by variables $\mathbf{r}^i$, i 1, N.

Establishing elementary equilibrium equations at each element tip between equilibrium nodal forces and the two inter-element forces on each side, and making a simple trivial count, one obtains that there are $2N$ unknown variables while only $2N-2$ linear independent equilibrium equations. So, the inter-element forces are undetermined and their values depend on two arbitrary parameters, which for the sake of convenience are

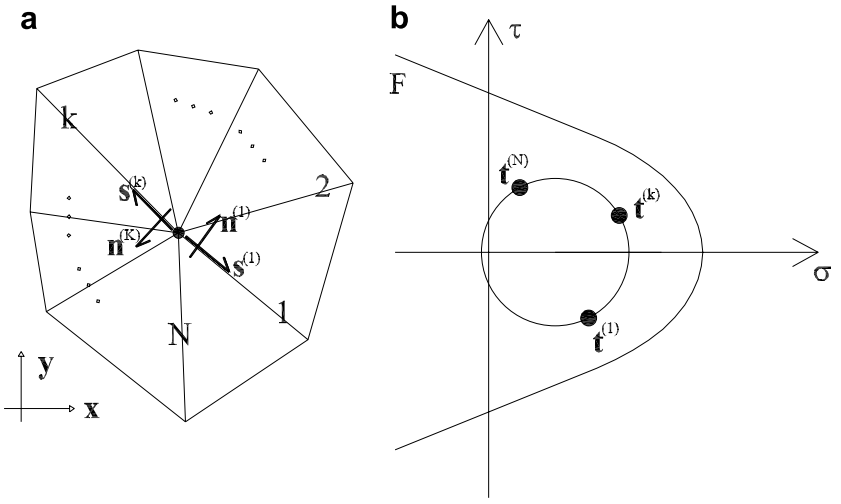

Fig. 4. (a) Elements and mesh lines around a corner node, with representation of the local reference normal and tangential unit vectors; (b) stress state at the node before stresses at any line have reached the cracking surface (“Stage 0”).

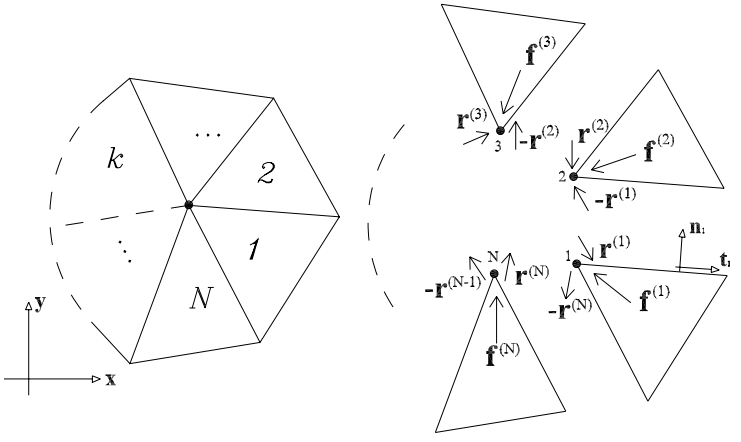

Fig. 5. Equilibrated nodal (**f**) and inter element (**r**) forces at an interior corner node in a homogeneous medium.

chosen equal to the components of one the inter-element force vectors denoted as **r**. Now, a procedure is established to determine these two arbitrary variables.

The inter-element forces, initially unknown, are directly related to the *inter-element stresses* or stress tractions $\mathbf{t}^{(i)}$ via the contributing area concept:

$$\mathbf{t}^{(i)} = \begin{pmatrix} \sigma^{(i)} \\ \tau^{(i)} \end{pmatrix} = \frac{1}{\Omega^{(i)}} \mathbf{Q}^{(i)} \begin{pmatrix} r_x^{(i)} \\ r_y^{(i)} \end{pmatrix} \tag{8}$$

where $\Omega^{(i)}$ stands for the contributing area for line (i) (these areas can be determined using the principle of virtual work in a way similar to the standard procedure to calculate nodal forces equivalent to external distributed forces), and $\mathbf{Q}^{(i)}$ for the rotation matrix from the global (**x**,**y**) to the local ($\mathbf{n}^{(i)}$,$\mathbf{s}^{(i)}$) reference system.

At the same point (corner node), an (a priori unknown) nodal stress tensor **T** is defined, and the following minimization function is considered:

$$\Phi = \sum_{i\ 1}^{N} \left((\sigma^{(i)} - \mathbf{n}^{(i)} \cdot \mathbf{T} \cdot \mathbf{n}^{(i)})^2 + (\tau^{(i)} - \mathbf{s}^{(i)} \cdot \mathbf{T} \cdot \mathbf{n}^{(i)})^2 \right) \tag{9}$$

in which the differences between the equilibrated stress tractions (obtained by Eq. (8)) and the projections of the (unknown) nodal stress tensor, in the normal and tangential directions, are squared and summed for all the mesh lines converging onto the corner node. Note that, by virtue of previous Eq. (9) and of the nodal equilibrium equations, the inter-element equilibrated stress tractions may be ultimately expressed in terms of the two scalar variables contained in the arbitrary indeterminate vector $\bar{\mathbf{r}}$. Therefore, the scalar function in Eq. (9) depends on the three components of $\mathbf{T}$ and the two components of $\bar{\mathbf{r}}$.

The missing equations are obtained by double minimization of Φ. First, it is assumed that the arbitrary force $\bar{\mathbf{r}}$ is known, and the values of the components of the nodal stress tensor $\mathbf{T}$ that minimize Φ are obtained by setting equal to zero the derivatives of Φ with respect to those same three components. This has to be done in closed form, since the arbitrary force is actually not known in advance, and the resulting expressions are functions of those two arbitrary force components. Then, from the three new equations obtained, the components of the nodal stress tensor are isolated and substituted back into the expression of Φ (9), so that the minimization function becomes actually a function of the two components of $\bar{\mathbf{r}}$ only. Then a second minimization of the function is performed, also in closed form, this time with respect to the two components of the arbitrary inter-element force $\bar{\mathbf{r}}$.

The result of the above derivation turns out surprisingly simple, leading to the linear system:

$$\mathbf{D} \cdot \mathbf{r} - \mathbf{d} = \mathbf{0} \tag{10}$$

from which the values of the $\mathbf{r}$ components can be easily obtained as the solution of a 2×2 linear system. From these, using previous equations one can recover all the inter-element forces and stresses, as well as the nodal stress tensor. The values obtained in this way have been verified in several examples, and turn out to be always exact for a uniform stress state (i.e. the nodal stress tensor coincides with the prescribed stress state on the overall mesh, and the stress tractions all sit on the corresponding Mohr circle, e.g. see Fig. 4b). For a non-uniform stress state, the stress tractions may not sit exactly on the circle, the circle itself may not coincide exactly with the expected stress state. However, they represent the best fit possible by the least square criteria employed, depending on the degree of refinement of the mesh and on the approximation order of the finite elements used (linear, quadratic, etc.). In any case, the overall accuracy always turns out to be equal (at least) or (generally) better than results obtained with alternative available techniques such as stress average smoothing. In the reference paper [19], the above theory is also extended to corner nodes on the domain boundary, as well as on the interface between two materials.

3.2. Stage 1: cracking criterion reached for one single line

The previous derivation to obtain inter-element tractions is only valid while all of the resulting stress tractions on the mesh lines converging onto the corner node, remain inside the cracking criterion in Mohr space, as for instance depicted in Fig. 4b.

But for increasing external loads, eventually, one of the lines will reach the failure criterion. For the first line crack at the first node in the FE mesh, this *contact point* may be easily located by numerical (e.g. midpoint algorithm) or analytical procedures (e.g. see closed-form solutions for contact points in hyperbolic loading surfaces in [23]), leading to the specific value of the external loading factor μ_1, for which this takes place.

From this point on, for an increasing external loading factor, the formulation must change, since otherwise the cracking criterion would be exceeded at that crack line, something it was assumed not possible in Section 2.3.

On the other hand, the question may arise whether at this point a crack may already open through the corner node. This is, however, not possible since kinematic compatibility at the node implies that, if two element tips detached from each other, two (and not only one) lines at least would have to exhibit crack opening and therefore also would have to have reached the cracking criterion, which at this ''stage 1'' is not the case yet. The situation is represented in Fig. 6, where the stress traction on one of the lines is already on the cracking surface while the others are not.

For increasing external loading factor beyond the first contact point ($\mu > \mu_1$), the stress tensor at the node and the corresponding line tractions must still grow, except for the mesh line for which the cracking criterion has been reached, for which stress tractions are subjected to the condition:

$$F(\mathbf{t}^{(k)}) = 0 \tag{11}$$

which means that they can remain constant or "slide" on the cracking surface. In this way, the previous condition acts as a constraint on the double minimization formulation previously developed for "stage 0", which otherwise is still applicable in this case.

One way to introduce this constraint into the formulation without the need of Lagrange multipliers, consists of:

(i) choosing the arbitrary inter-element force as that corresponding to the line for which the cracking criterion has been reached, i.e. $\mathbf{r} = \Omega^{(k)}\mathbf{Q}^{(k)} \cdot \mathbf{t}^{(k)}$,
(ii) using a specific cracking criterion expression to relate the two components of the stress traction on that line, and therefore reduce the arbitrary variables from two (the components of $\mathbf{r}$ in the global reference system $\mathbf{x}$, $\mathbf{y}$) to one (one component of the stress traction).

Using the hyperbolic cracking criterion of Section 2.3, Eq. (7), the tractions laying on the fracture surface F may be expressed in vector form as:

$$\mathbf{t}^{(k)} = \begin{bmatrix} \sigma(\tau) \\ \tau \end{bmatrix} = \begin{bmatrix} \frac{1}{\tan\phi}\left(c - \sqrt{(\tau)^2 + (c - \chi\tan\phi)^2}\right) \\ \tau \end{bmatrix} \tag{12}$$

which means that the only arbitrary variable in the system is now the shear component $\tau^{(k)}$ at the line having reached the cracking criterion, which for convenience has been renamed as τ.

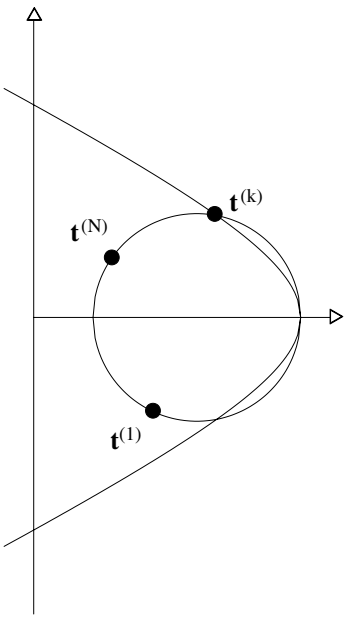

Fig. 6. Stage 1: cracking criterion reached by one single traction, $\mathbf{t}^{(k)}$, while the other mesh lines tractions are far from the fracture surface F.

By using previous relation in Eq. (8), the original arbitrary forces $\mathbf{r}$ may also be expressed in terms of the only unknown τ:

$$\mathbf{r} = \Omega^{(k)}\mathbf{Q}^{(k)}\mathbf{t}^{(k)} = \Omega\mathbf{Q}\begin{bmatrix}\sigma(\tau)\\ \tau\end{bmatrix} \tag{13}$$

and therefore all the remaining $N-1$ inter-element forces and stresses may also be expressed in terms of the same single arbitrary variable $\boldsymbol{\tau}$.

Under these conditions, the same objective function Φ as in previous subsection (9) is considered, although now it only needs to be minimized with respect to τ. This is done by using the chain rule:

$$\frac{\partial\Phi}{\partial\tau} = \frac{\partial\Phi}{\partial\mathbf{r}}\frac{\partial\mathbf{r}}{\partial\tau} = 0 \tag{14}$$

The last term of previous equation, renamed for simplicity $\mathbf{r}'$, may be simply evaluated by differentiation of (13):

$$\frac{\partial\mathbf{r}}{\partial\tau} = \mathbf{r}' = \Omega\mathbf{Q}\begin{bmatrix}\frac{\partial\sigma}{\partial\tau}\\ 1\end{bmatrix} = \Omega\mathbf{Q}\begin{bmatrix}-\frac{\tau}{\tan\phi\sqrt{\tau^2+(c-\chi\tan\phi)^2}}\\ 1\end{bmatrix} \tag{15}$$

Taking into account now that the derivative of Φ with respect to $\mathbf{r}$ is the same as in Section 3.1, Eq. (10), previous Eq. (14) can be finally written in final form as:

$$\frac{\partial\Phi}{\partial\tau} = \mathbf{r}'^{T}\cdot\mathbf{D}\cdot\mathbf{r} - \mathbf{r}'^{T}\cdot\mathbf{d} = 0 \tag{16}$$

This actually constitutes a scalar equation from which the value of τ can be obtained. Once τ is known, the inter-element forces of all the mesh lines around the corner node can be computed using Eq. (13) and the nodal equilibrium equations.

3.3. Stage 2: cracking criterion reached for two mesh lines at the node

The derivation presented for "stage 1" in previous section, is valid as long as only one line converging on that node has reached the cracking criterion while the others still have not. But of course, if external loading factor μ keeps increasing (and lets remember here that from the structural/FE viewpoint this is still a linear elastic calculation, since no cracks have opened yet), the cracking criterion will eventually be also satisfied for a second potential crack line. Similar to previous section, the new contact point may be located by numerical or analytical procedures, leading to the specific value of the external loading factor μ_2 for which this second contact takes place.

From this point on, for an increasing external loading factor, the formulation must change, since otherwise the cracking criterion would be exceeded at that second crack line, something it was assumed not possible in Section 2.3.

On the other hand, the question may arise again whether at this point, with two lines converging on the same node having reached cracking criterion, a crack may already open through the corner node and be "visible" at the structural/FE. However, in the general case these conditions are still not sufficient for crack opening, due to the flow rule assumptions defined together with the cracking criterion in Section 2.3. The flow rule defines the direction of the opening for each of the cracks independently and it must also be satisfied simultaneously by the two cracks. As it is illustrated in Fig. 7, the coincidence of the flow rule for the two cracking lines in a global coordinate system is not automatically ensured only by the fact that the cracking criterion is met for both of them. In fact, calculations show that in general this is not the case which means that, in spite of satisfying the failure conditions for both lines, the crack cannot open yet due to kinematic incompatibility.

This situation of two concurring crack lines in failure state but without being able to open, will be maintained until the flow rules get realigned, which in general will take place for a higher loading factor $\mu_3 > \mu_2$.

The formulation for evaluating inter-element forces and stresses during "stage 2" with $\mu_2 < \mu < \mu_3$, does not require any minimization. As already said in previous subsections, basic equilibrium at each element tip

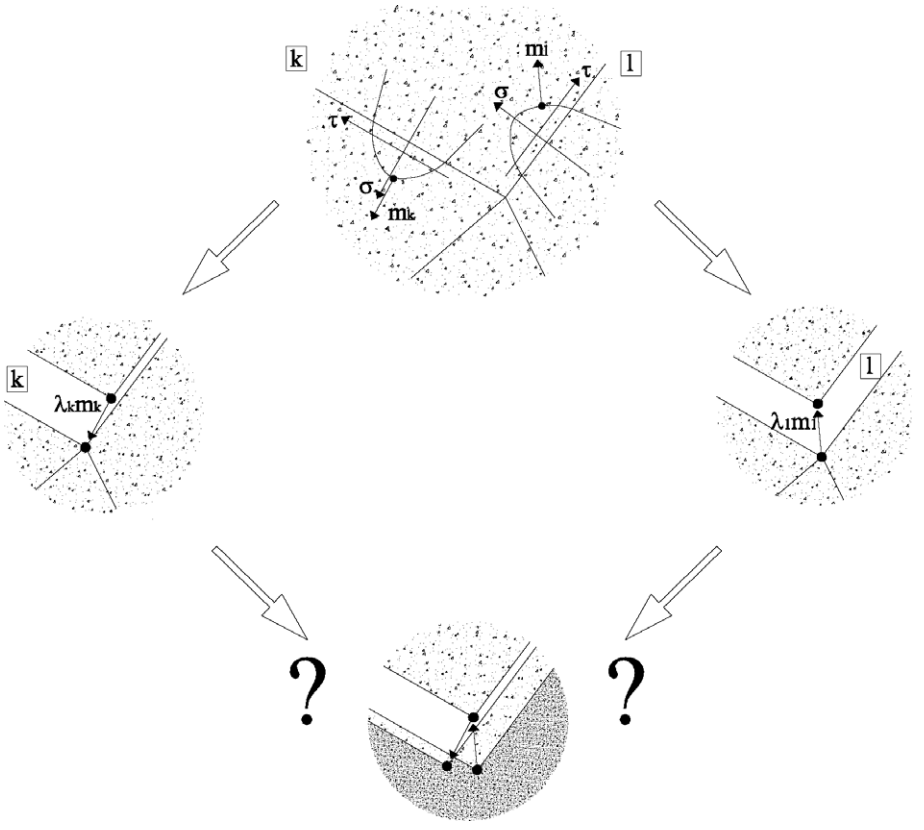

Fig. 7. Stage 2: kinematic incompatibility between the crack lines k and l; they have reached the "stage 2" but they can still not produce the opening of a crack.

between equilibrated nodal forces obtained from the FE analysis and inter-element forces, provide $2N-2$ equations. The cracking criterion applied to the two cracking lines provides two additional equations, totaling $2N$, which coincides with the number of the unknown components (two for each of the N inter-element forces or stresses).

One procedure to solve the system is to write the hyperbolic failure criterion in Eq. (7) for each of the cracking lines denoted by indices k and l:

$$(\tau^{(k)})^2 = (c - \sigma^{(k)} \tan\phi)^2 - \tau_0^2 \tag{17}$$

$$(\tau^{(l)})^2 = (c - \sigma^{(l)} \tan\phi)^2 - \tau_0^2 \tag{18}$$

in which for convenience the new constant $\tau_0 \quad c - \chi\tan\phi$ has been introduced.

Using Eq. (13), the $2N-2$ independent equations of equilibrium of the nodal forces can be rewritten in terms of N nodal inter-element stresses $\mathbf{t}^{(i)} \quad \sigma^{(i)},\tau^{(i)}$. Adding to this system the two failure criterion equations (Eqs. (17) and (18)) for the cracking lines l and k, one gets a non-linear system whose number of unknown is equal to the number of equations, and that, for this reason, may be solved in closed form.

Note that the system coefficients involve the equilibrated FE forces on the concurrent element tips, and therefore the entire solution depends on the overall loading factor μ. Due to the non-linearity (irrationality) of the system, it admits four roots that may be real or complex (from the various numerical simulations performed to verify the formulation, it has been observed that in general the system exhibits two complex and two real roots, although at this point this cannot be proven to be a general rule). Among the real roots (only ones with physical meaning) the one closer to the value of the stresses computed in the previous increment $\Delta\mu$ is taken as the correct one. Obviously, the stress tractions obtained on the two lines at cracking state will automatically satisfy the cracking criterion imposed via the above equations.

3.4. Stage 3: Onset of crack opening

The formulation developed for stage 2 will be valid only until the kinematic compatibility for crack opening is achieved. This may actually happen in two ways:

(1) the stress tractions for one or more of the remaining mesh lines (other than the two already on the cracking surface) also reach the cracking condition $F(\mathbf{t}^{(i)} \quad 0)$, or
(2) the flow rules of the two cracking lines become parallel.

In the first case, i.e. if one (or more) additional line(s) reaches the cracking criterion before the flow rules of the two original cracking lines of stage 2 become parallel, the onset of cracking is actually reached on the only condition that the various flow rules constitute a set of linearly dependent vectors. This can be easily understood by considering that once the cracks start opening, kinematic compatibility requires that the sum of the various relative displacements for each opening crack should be zero. Given the arbitrary value of the inelastic multipliers, the satisfaction of this condition is practically ensured with three or more opening cracks, except if some of the flow rules would happen to be parallel, which could cause the remaining one to be linearly independent from the rest. This could happen for instance in a triple crack if two of the cracking lines are on opposite sides of the node and have the same orientation (in which case in practice they could be considered as a single 'through' crack line). Except in these special situations, when a third line reaches cracking conditions the onset of cracking at the node is usually attained.

If the second condition above is satisfied first (i.e. the flow rules of the two cracking lines from stage 2 become parallel before any other line reaches the cracking criterion), that also marks the onset of cracking at the node. The opening crack is composed of the two cracking lines, which in general are not aligned and therefore the opening crack will exhibit a kink at the node, see Fig. 8.

The identification of the precise loading factor μ_3 for which this second condition takes place may be done in two ways:

(1) *via incremental computations*, i.e. by increasing the external loading factor by small steps, repeating each time the calculations of stage 2 and verifying the direction of the corresponding flow rules until they coincide, or
(2) *via limit analysis*.

The step-by-step procedure does not deserve any further explanation beyond what was already presented in the previous section. However, one numerical observation is that in the results obtained in different examples, when the loading factor μ attains the value of μ_3, the real roots of the system coincide, and this avoids having to choose among the various roots of the system.

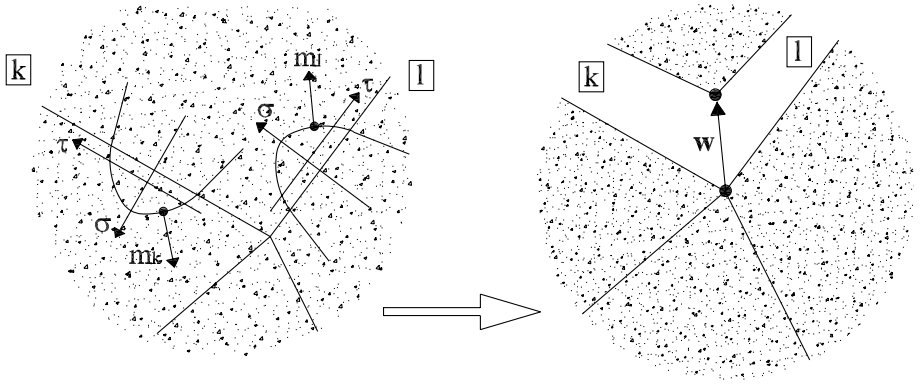

Fig. 8. Stage 3: kinematic compatibility for crack opening; the flow vectors $\mathbf{m}_k$ and $\mathbf{m}_l$ are parallel.

Concerning the procedure for limit analysis, that is similar to the one used for the incremental analysis, with the difference that one new variable is introduced to the system, and as a consequence also one new equation. The variable is the loading factor μ, and the equation is the parallelism condition between the flow rule vectors $\mathbf{m}$ of the cracking lines. The value of μ obtained in this way is the one that satisfies simultaneously the parallelism condition of the flow rule vectors (kinematic compatibility for crack opening), the cracking criterion and the nodal equilibrium equations.

The flow rule vector $\mathbf{m}$ along each cracking line is not a unit vector (i.e. $\|\mathbf{m}\| \neq 1$), and it is written in the local reference system of each crack line ($\mathbf{n}$, $\mathbf{s}$). Considering the fracture surface presented in Eq. (7), the associated flow rule is:

$$\mathbf{m} = \begin{bmatrix} \frac{\partial F}{\partial \sigma} \\ \frac{\partial F}{\partial \tau} \end{bmatrix} = \begin{bmatrix} 2\tan\phi(c - \sigma\tan\phi) \\ 2\tau \end{bmatrix} \tag{19}$$

or, clearing the stress vector $\mathbf{t}$ in the previous formula, it becomes:

$$\mathbf{m} = \begin{bmatrix} -2\tan^2\phi & 0 \\ 0 & 2 \end{bmatrix} \begin{bmatrix} \sigma \\ \tau \end{bmatrix} + \begin{bmatrix} 2c\tan\phi \\ 0 \end{bmatrix} = \mathbf{A}\cdot\mathbf{t} + \mathbf{b}. \tag{20}$$

In order to compare the flow rule vectors of two different lines, they have to be both rotated to the global reference system $\mathbf{x}$, $\mathbf{y}$:

$$\tilde{\mathbf{m}}(\mathbf{x},\mathbf{y}) = \mathbf{Q}\cdot\mathbf{m}(\mathbf{n},\mathbf{s}) \tag{21}$$

Finally, the parallelism condition can be expressed as:

$$\frac{\tilde{m}_x^{(l)}}{\tilde{m}_y^{(l)}} - \frac{\tilde{m}_x^{(k)}}{\tilde{m}_y^{(k)}} = 0 \tag{22}$$

As previously said, the solving system is composed by $2N - 2$ nodal equilibrium equations (that can be written in terms of stresses or forces), two consistency conditions ($F(\mathbf{t}^{(i)})$ 0) for the two cracking lines presented in Eqs. (17) and (18), and the parallelism condition of Eq. (22).

Even in this case the non-linearity of the system leads to the multiplicity of the solution. Among the real roots of the system, the smaller value of μ within those that are greater than μ_2 is taken as the correct one.

Independently of following the limit or the incremental analysis, when the flow rule coincidence is detected, stage 3 is achieved and the real opening of the crack becomes possible at FE level, marking the end point of the current study.

Note that when two of the mesh lines have the same orientation and are located on opposite sides of the node, a straight crack becomes possible, and stage 2 and 3 happen at the same time, i,e. when failure conditions are achieved for the second crack, at the same time flow rules turn out to be just parallel and the onset of crack opening is reached. In a similar way, under special conditions of geometrical and loading symmetry, it may happen that failure conditions are reached simultaneously for two crack lines, and so stage 1 and 2 would merge as well. But under general conditions, the three stages should exist, as it will be illustrated in the following application examples.

4. Examples

4.1. Example 1

The first example of application consists of the mesh and loads depicted in Fig. 9. The "corner nodes" under study are the central node number 7 to which four potential crack lines converge, and nodes number 4, 5, 9 and 10, to which three potential cracking lines concur. The mesh is made by linear triangles elements, which are assumed linear elastic. The mechanical parameters of the elastic continuum are: E 1000 MPa and v 0.2. The specimen is 14 mm wide and 18 mm high. The boundary conditions are represented on the left side of Fig. 9. The uniform stress state applied along the vertical direction is twice the stress along the hori-

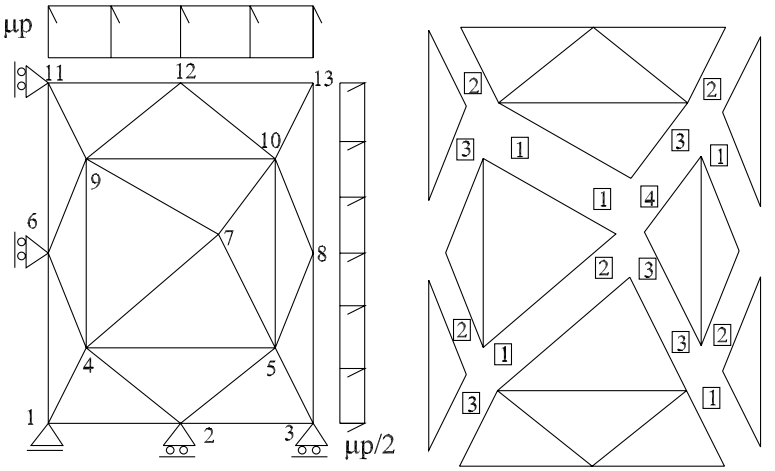

Fig. 9. On the left: mesh composed by linear triangular elements, boundary conditions and numeration of nodes; on the right: the potential cracking lines around nodes 4, 5, 7, 9 and 10 are explicitly represented and numbered.

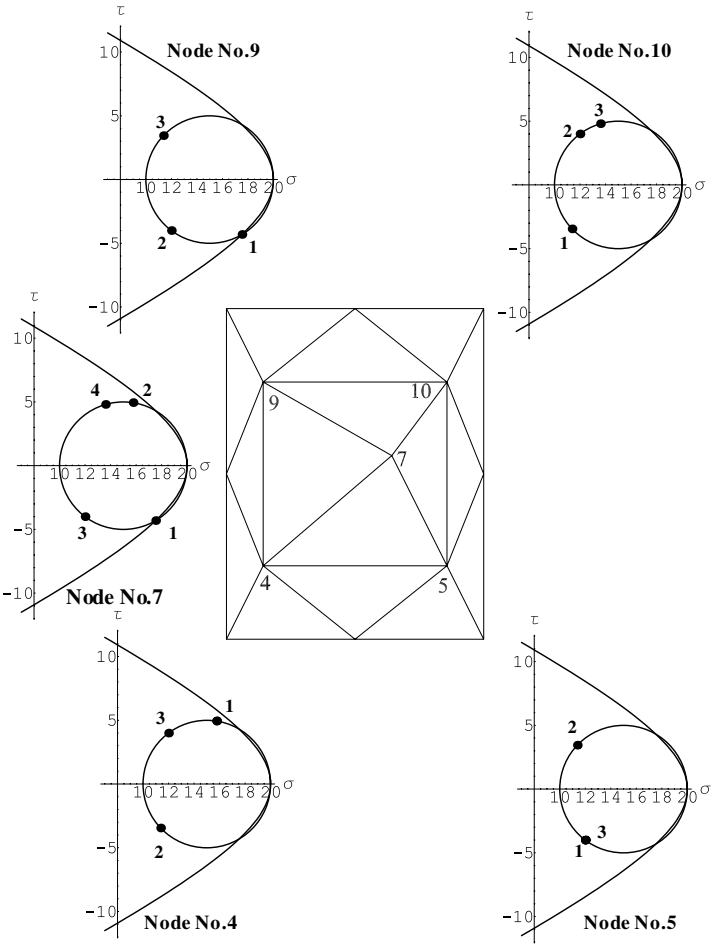

Fig. 10. Stage 1 for node 7 and 9 (one of the potential cracking lines satisfies the cracking criterion); stage 0 for nodes 4, 5 and 10 (the stresses along the cracking lines are inside the rigid domain).

zontal direction. The loading factor μ rules the increment of the applied load, whose nominal value is p_0 20 MPa. The analysis is performed in plane stress.

On the right side of Fig. 9, the potential cracking lines of the mesh are explicitly represented. The cracking criterion for these lines is the one presented in Section 2.3. The parameters of the hyperbolic failure criterion are: χ 20 MPa, c 16.92 MPa and $\tan\phi$ 0.5. The other lines concurrent to nodes 4, 5, 9 and 10 are not taken into consideration as cracking lines. As it will be seen, the most critical node that in the end will reach onset of cracking first is the central node No. 7. Attention will be focused mainly on this node, although reference will also be made to what happens in other nodes.

4.1.1. Stage 1: cracking criterion attained by one cracking line

For the loading factor value of μ 1.0, the cracking surface is reached by the stress traction on line 1 at node 7, as well as on line 1 at node 9. The tractions along the other lines in the mesh stay inside the cracking criterion. The results at this stage are shown in Fig. 10.

4.1.2. Stage 2: cracking criterion attained by two cracking lines

For μ 1.058855857 the situation at node 7 is the following: the traction vector of the cracking line number 1 has been moving tangentially to the fracture surface until the tractions of the cracking line number 4 have satisfied the cracking criterion too. This state represents the end of stage 2 for node 7 (as showed in Fig. 11)

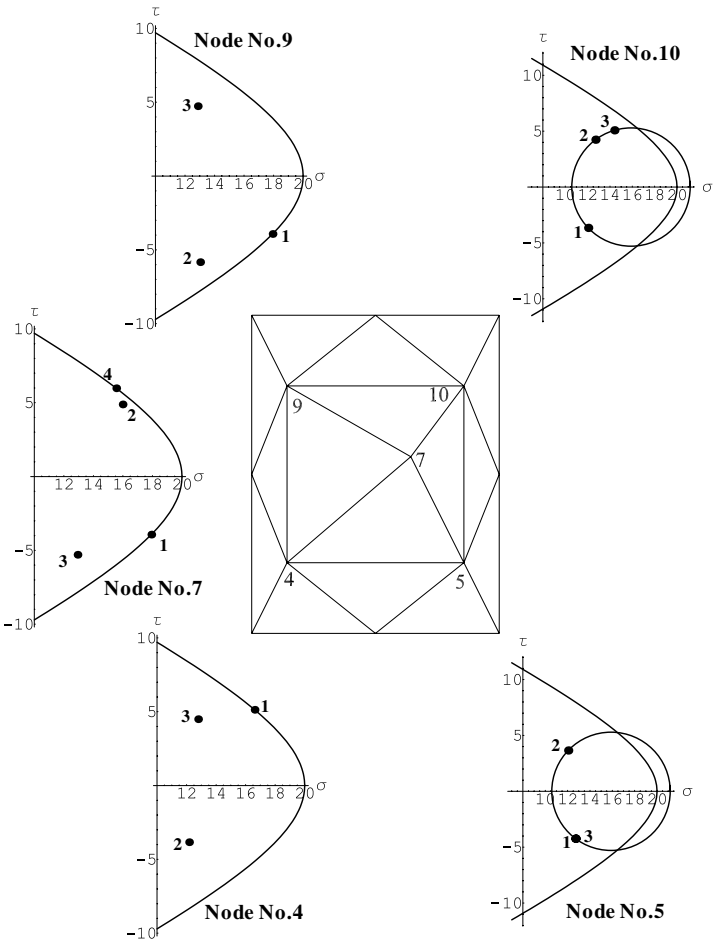

Fig. 11. Stage 2 for node 7 (the tractions of two cracking lines lay on the fracture surface, but they still no satisfy the kinematic compatibility for the opening of a crack); stage 1 for nodes 4 and 9; stage 0 for nodes 5 and 10.

At node 9 the stresses of line number 1 remains on the cracking criterion, but no other lines have reached the fracture surface for $1 < \mu < 1.058855857$.

At node 4, for μ 1.04955768385, the stresses on line number 1 attained the cracking criterion, and until μ 1.058855857 no other lines have reached this condition.

At nodes 5 and 10 no lines have reached the cracking criterion.

4.1.3. Stage 3: kinematic compatibility conditions attained

For μ 1.067790745, node 7 reaches the onset of cracking condition (stage 3) since the flow vectors of the cracking line 1 and 4 concurrent at this node become parallel. Nodes 4 and 9 remain in stage 1, and nodes 5 and 10 in stage 0. All this is represented in Fig. 12.

This point would indicate the beginning of the non-linear analysis with one opening crack, and therefore marks the end of the current study devoted to clarify the conditions and stages until crack opening may occur.

Note that for the whole range between μ 0 and onset of nodal crack opening μ 1.067790745, the stress state at the Gauss points of the continuum triangular elements is uniform and equal to the external applied load (σ_x $\mu p/2$,σ_y μp). In contrast, during this loading process and after μ 1.0, the stress tractions along mesh lines that are potential cracks undergo some redistribution as the cracking criterion is progressively reached. This has been shown by the different values of tractions at the nodes of the same mesh line for the same loading factor increment.

4.2. Example 2

This second application example consists of the mesh and loads depicted in Fig. 13. The "corner nodes" under study are nodes 4, 5 and 6 in the center of the mesh, each with three potential crack lines. The mesh is made by linear triangles elements, which are assumed linear elastic. The mechanical parameters of the elastic continuum are: E 1000 MPa and ν 0.2. The specimen is 13 mm wide and 14 mm high. The boundary

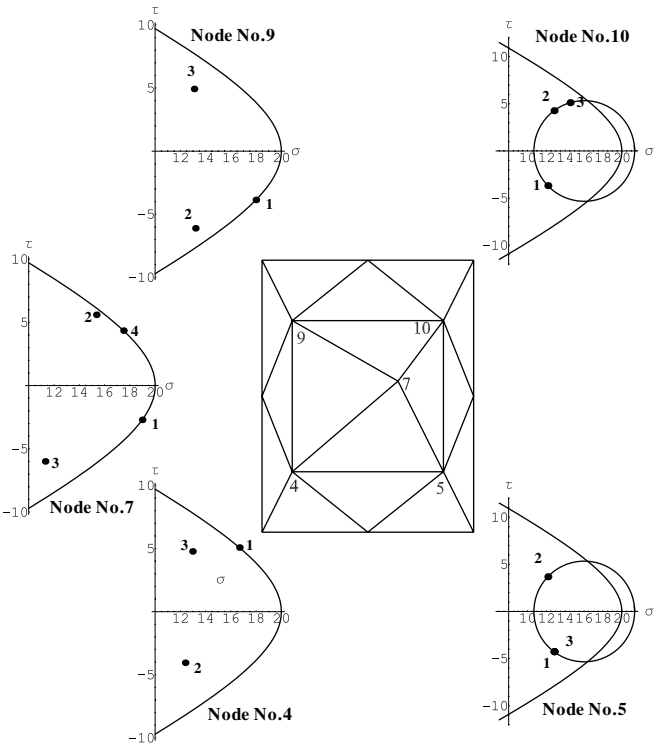

Fig. 12. Stage 3 for node 7 (the flow rule vectors of the cracking line number 1 and 4 are parallel); stage 1 for nodes 4 and 9; stage 0 for nodes 5 and 10.

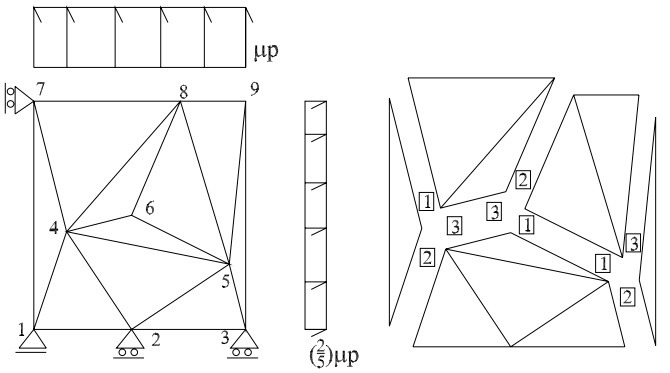

Fig. 13. On the left: mesh composed by linear triangular elements, boundary conditions and node numbers; on the right: the potential cracking lines around nodes 4, 5, and 6 are explicitly represented and numbered.

conditions are represented on the left side of Fig. 13. The uniform stress state applied along the horizontal direction is $\frac{2}{5}$ the stress along the vertical direction. The loading factor μ rules the increment of the applied load, whose nominal value is p_0 50 MPa. The analysis is performed in plane stress.

On the right side of Fig. 13, the potential crack lines of the mesh are explicitly represented. The cracking criterion assigned to these is the one presented in Section 2.3. The parameters of the hyperbolic failure criterion are: χ 50 MPa, c 43.46 MPa and $\tan\phi$ 0.5 The other lines concurrent to nodes 4, and 5 are not taken into consideration as cracking lines. This example is presented to show the particular situation in which two cracking lines can simultaneously satisfy the cracking criterion, but not the kinematic conditions. For this reason, attention will be focused mainly on node No. 6, although reference will also be made also to what happens in other nodes.

4.2.1. Stage 1 + 2: cracking criterion attained by two cracking lines simultaneously

For the loading factor value of μ 1.0, the cracking surface is simultaneously reached by the tractions on line 1 and 3 at node 6. Consequentially also cracking line 3 at node 4 and cracking line 1 at node 5 satisfy the cracking criterion. The results at this stage are shown in Fig. 14.

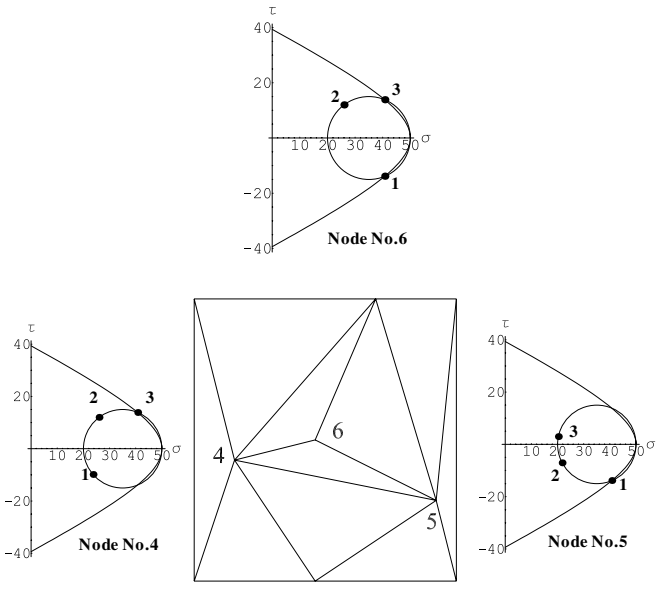

Fig. 14. Stage 1 + 2 for node 6 (two potential cracking lines satisfy simultaneously the cracking criterion); stage 1 for nodes 4 and 5 (only one cracking line lay on the fracture surface).

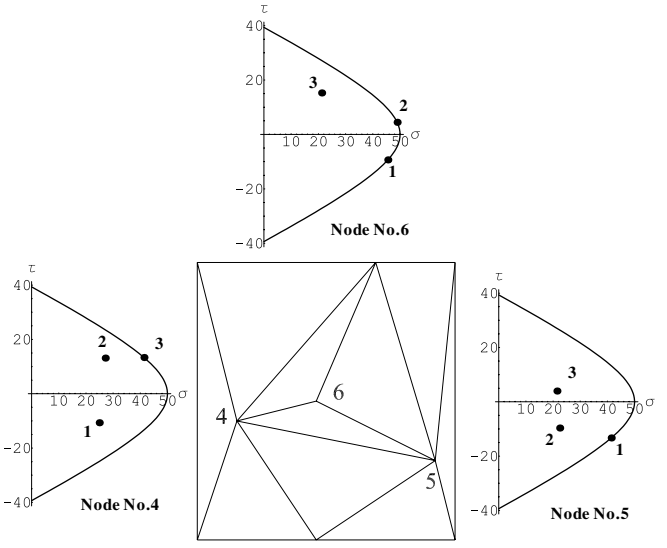

Fig. 15. Stage 3 for node 6 (the flow rule vectors of the cracking line number 1 and 3 are parallel); stage 1 for nodes 4 and 5.

4.2.2. Stage 3: kinematic compatibility conditions attained

For μ 1.03628384281, node 6 reaches the onset of cracking condition (stage 3) since the flow rule vectors of crack lines 1 and 3 at that node become parallel. Nodes 4 and 5 remain in stage 1. All this is represented in Fig. 15.

5. Summary and concluding remarks

In this paper, a study on the conditions for crack opening along mesh lines concurring on a FE "corner node" is presented. The study is carried out in the context of a general research line pursuing the development of new analysis methods for fracture and cracking along mesh lines, which would not require to introduce double-node interfaces along all mesh lines from the beginning of the analysis, but at the same time would verify cracking conditions at "corner nodes" rather than only at "middle nodes" of quadratic elements as in existing literature. The study is a follow up of recent work published by the authors, in which a double minimization method was developed for the calculation of stress tractions along mesh lines concurrent on a corner node. In this case, a cracking criterion and flow rule are established for the mesh lines; different cases are distinguished and formulations developed depending on whether those conditions are reached for none (stage 0), one (stage 1), or two mesh lines (stage 2) and, in that case, whether the onset of nodal crack opening (stage 3) is reached, either by opening of a third crack, or by the two flow rules becoming parallel.

Two simple examples of application have been given, illustrating some of the situations which can take place at nodes with three or four potential crack lines. The results can be however extrapolated easily to nodes with more mesh lines. All four stages of the cracking process occur sequentially, for increasing loading factors. Overall, the study shows the richness and complexity of the cracking conditions at mesh lines and nodes, that unfolds from post-processing of simple linear elastic calculations with the standard displacement-based FE method, and a standard hyperbolic crack failure criterion. The results obtained clarify sufficiently the main points under study, and open the door for further developments towards the main goal of the general research line stated above.

Acknowledgements

The first author wishes to thank the support received from MUIR (Italy) and Generalitat de Catalunya (Barcelona) for the development of her doctoral thesis. The second author acknowledges research Grants

MAT2003-02481 from MEC (Madrid) and 2005SGR00842 from Generalitat de Catalunya. Research project 2004/33 from MFOM (Madrid) is also gratefully acknowledged.

References

[1] Ngo D, Scordelis AC. Finite element analysis of reinforced concrete beams. J Am Concrete Inst 1967;64(14):152–63.
[2] Bažant ZP, Oh BH. Microplane model for progressive fracture of concrete and rock. ASCE J Engng Mech 1985;111:559–82.
[3] Bažant ZP. Mechanics of distributed cracking. Appl Mech Rev 1986;39(5):675–705.
[4] Willam K, Pramono E, Sture S. Fundamental issues of smeared crack models. In: Shah SP, Swartz SE, editors. SEM-RILEM international conference on fracture of concrete and rock. Bethel, Connecticut: Society of Engineering Mechanics; 1987. p. 192–207.
[5] Rots JG. Computational Modeling of Concrete. PhD thesis. TU Delft; 1988.
[6] Ingraffea AR, Saouma VE. Numerical modelling of dicrete crack propagation in reinforced and plain concrete. In: Sih GC, DiTomasso A, editors. Fracture mechanics of concrete. Dordrecht, The Netherlands: Martinus Nijhiff; 1985. p. 171–225.
[7] Bittencourt TN, Ingraffea AR, Llorca J. Simulation of arbitrary, cohesive crack propagation. In: Bažant ZP, editor. Fracture mechanics of concrete structures (FRAMCOS1). Breckenridgr, Colorado: Elsevier; 1992. p. 171–225.
[8] Belytschko T, Black T. Elastic crack growth in finite elements with minimal remeshing. Int J Numer Meth Engng 1999;45:601–20.
[9] Oliver J, Cervera M, Manzoli O. Strong discontinuities and continuum plasticity models: the strong disontinuity approach. Int J Plasticity 1999;15:319–51.
[10] Rots JG, Schellekens JCJ. Interface elements in concrete mechanics. In: Bićanić N, Mang H, editors. Computer-aided analysis and design of concrete, Vol. 2. Zell-am-See, Austria: Pineridge Press; 1990. p. 909–18.
[11] Camacho GT, Ortiz M. Computational modelling of impact damage in brittle materials. Int J Solids Struct 1996;33(20–22):2899–938.
[12] Lopez CM, Carol I. Numerical analysis of concrete microstructure using interface elements. Anales de Mecanica de la Fractura 1995;12:75–80.
[13] Carol I, Lopez CM, Roa O. Micromechanical analysis of quasi-brittle materials using fracture-based interface elements. Int J Numer Meth Engng 2001;52(1/2):193–215.
[14] Sluys LJ, Berends AH. 2D/3D modelling of crack propagation with embedded discontinuity elements. Computational Modelling of Concrete Structures (EURO–C). Austria: Badgastein; 1998. p. 399–408.
[15] Dugdale DS. Yielding of steel sheets containing slits. J Mech Phys Solids 1960;8:100–4.
[16] Hillerborg A. A model for fracture analysis. Technical Report TVBM-3005, Division of Building Materials, The Lund Institute of Technology (Lund, Sweden); 1978.
[17] Caballero A, Carol I, López. 3D meso-structural analysis of concrete specimens under uniaxial tension. Comput Meth Appl Mech Engng 2006;195(52):7182–95.
[18] Ortiz M, Pandolfi A. Finite-deformation irreversible cohesive elements for the three-dimensional crack-propagation analysis. Int J Numer Meth Engng 1999;44(9):1267–82.
[19] Ciancio D, Carol I, Cuomo M. On inter-element forces in the FEM-displacement formulation, and implications for stress recovery. Int J Numer Meth Engng 2006;66(3):502–28.
[20] Carol I, Prat PC, Bažant ZP. New explicit microplane model for concrete: theoretical aspects and numerical implementation. Int J Solids Struct 1992;29(9):1179–91.
[21] Carol I, Bažant ZP. Damage and plasticity in microplane theory. Int J Solids Struct 1997;34(29):3807–35.
[22] Carol I, Prat PC, López CM. A normal/shear cracking model. Application to discrete crack analysis. ASCE J Engng Mech 1997;123(8):765–73.
[23] Gens A, Carol I, Alonso EE. An interface element formulation for the analysis of soil-reinforcement interaction. Comput Geotech 1988;7:133–51.